Title

An inverse radiation model for optical determination of temperature and species concentration: Development and validation

Authors

Ren, T
Modest, MF
Fateev, A
et al.

Publication Date

2015

DOI

10.1016/j.jqsrt.2014.10.005

Peer reviewed

Journal of Quantitative Spectroscopy & Radiative Transfer 151 (2015) 198–209

Contents lists available at ScienceDirect

Journal of Quantitative Spectroscopy & Radiative Transfer

journal homepage: www.elsevier.com/locate/jqsrt

An inverse radiation model for optical determination of temperature and species concentration: Development and validation

Tao Ren [a], Michael F. Modest [a,*], Alexander Fateev [b], Sønnik Clausen [b]

[a] School of Engineering, University of California, Merced, CA, USA
[b] Department of Chemical and Biochemical Engineering, Technical University of Denmark, 2800 Kgs. Lyngby, Denmark

ARTICLE INFO

Article history:
Received 10 April 2014
Received in revised form
2 October 2014
Accepted 5 October 2014
Available online 18 October 2014

Keywords:
Inverse radiation
Transmissivity
Temperature
Concentration
Carbon dioxide
Water vapor

ABSTRACT

In this study, we present an inverse calculation model based on the Levenberg–Marquardt optimization method to reconstruct temperature and species concentration from measured line-of-sight spectral transmissivity data for homogeneous gaseous media. The high temperature gas property database HITEMP 2010 (Rothman et al. (2010) [1]), which contains line-by-line (LBL) information for several combustion gas species, such as CO_2 and H_2O, was used to predict gas spectral transmissivities. The model was validated by retrieving temperatures and species concentrations from experimental CO_2 and H_2O transmissivity measurements. Optimal wavenumber ranges for CO_2 and H_2O transmissivity measured across a wide range of temperatures and concentrations were determined according to the performance of inverse calculations. Results indicate that the inverse radiation model shows good feasibility for measurements of temperature and gas concentration.

1. Introduction

Advanced optical diagnostics and multi-scale simulation tools will play a central role in the development of next-generation clean and efficient combustion systems, as well as in upcoming high-temperature alternative energy applications. Combustion diagnostics have reached high levels of refinement, but it remains difficult to make quantitatively accurate nonintrusive measurements of temperature and species concentrations in realistic combustion environments. Griffith et al. [2,3] were the first to recognize that measurements of the transmissivity or emissivity of rotational spectral lines of a gas can reveal its temperature. In order to extract temperature, a nonlinear least-square method was used to fit the integrated transmission minima. In their experiments, transmissivities for CO_2 10.4 μm and 9.4 μm bands at a fine resolution of 0.29 cm^{-1} for pure CO_2 [3] were measured. Best et al. [4,5] combined tomography and Fourier transform infrared (FTIR) spectrometer transmission and emission spectra to extract temperature, concentration and soot volume fraction fields. Not much detail was given, except that low resolution (32 cm^{-1}) scans were used. Song et al. [6–9] developed a spectral remote sensing technique to reconstruct temperature profiles in CO_2 mixtures based on radiative intensity measurements. In their experiments, spectra from 1.3 μm to 4.8 μm were imaged onto a 160-element lead selenide array detector. Spectral information only for the CO_2 4.3 μm band was used to retrieve the temperature profile and the spectral resolution is coarse and not changeable.

A number of gas property databases are available for transmissivity predictions, such as HITRAN 2008 [10] and HITEMP 2010 [1], which contain line-by-line (LBL) information

* Corresponding author.
E-mail address: mmodest@ucmerced.edu (M.F. Modest).

http://dx.doi.org/10.1016/j.jqsrt.2014.10.005
0022-4073/

for many gas species. HITEMP 2010, which is limited to only four species (CO_2, H_2O, CO and OH), contains data for "hot lines," which become active at high temperature. In the updated HITEMP 2010 CO_2 parameters were calculated from CDSD-1000 [11]. The database was extensively tested against measured medium-resolution spectra of CO_2 [12,13] for the 15, 4.3, 2.7, and 2.0 μm bands at temperatures of 300, 600, 1000, 1300, and 1550 K and measured high-resolution spectra of CO_2 in the 15, 4.3 and 2.7 μm bands at temperatures up to 1773 K [14]. The database was also tested against measured medium-resolution spectra of H_2O [15] for the 6.3, 2.7 and 1.8 μm bands at temperatures of 600, 1000, and 1550 K and measured high-resolution spectra of H_2O in the 2.7 and 1.8 μm bands at temperatures up to 1673 K [16]. Good agreement between measured and calculated spectra was found. In the present study, the predicted spectral transmissivities were calculated for different medium-to-coarse resolutions using rovibrational band spectra created from HITEMP 2010. Ideal FTIR instrument line shape (ILS) functions were used to convolve the high-resolution transmissivity spectra to generate different medium-to-coarse resolutions of FTIR transmissivity spectra for the CO_2 2.7 μm and 4.3 μm bands and H_2O 1.8 μm and 2.7 μm bands.

The goals of our research are to develop new radiation tools to accurately deduce temperature and species concentration profiles from radiometric measurements in laminar and turbulent combustion systems. As a start, in the present work inverse radiation tools for homogeneous gas media were developed to deduce temperature and concentration from higher to lower-resolution measurements of line-of-sight transmissivities. A number of inverse techniques have been used for temperature or concentration inversion. Several inverse radiation algorithms like the Quasi-Newton method [17], the Conjugate Gradient Method [18] and the Levenberg–Marquardt method [19] have been applied. From many transmissivity inversions, we found the Levenberg–Marquardt inverse scheme to be relatively reliable to retrieve temperature and concentration along single lines-of-sight, and to be more accurate and requiring less computational effort. Therefore, only the Levenberg–Marquardt method was employed in the scheme described below. The inverse model was validated by retrieving temperatures and concentrations from experimental medium-resolution CO_2 and H_2O transmissivity data obtained previously [12–16] for a wide range of temperatures and species concentrations.

2. Transmissivity measurements for CO_2 and H_2O

Bharadwaj and Modest performed measurements of CO_2 and H_2O transmissivity at temperatures up to 1550 K and with a resolution of $4\,cm^{-1}$ using a drop tube mechanism and FTIR spectrometer [12,13,15]. The gas temperature was measured by a thermocouple and a gas delivery system was used to supply mixtures of N_2+CO_2 and N_2+H_2O. By controlling the flow rate of N_2 and CO_2 or N_2 and H_2O, the desired mole fraction of CO_2 or H_2O in the test cell was obtained. CO_2 concentrations were measured by ball flow meters and H_2O concentrations were measured by an Agilent series micro-gas chromatograph. The reader is referred to [12,13,15] for more details on the experiment.

High-resolution transmissivity measurements have been made by Fateev and Clausen with an atmospheric-pressure high-temperature flow gas cell (HGC), Fig. 1, for CO_2 at temperatures up to 1773 K [14] and H_2O at temperatures up to 1673 K [16]. The gas cell was designed as a flow gas cell with a so-called "laminar flow window", where care was taken to obtain a uniform gas temperature profile and a well-defined path length. "Laminar flow window" is not an actual window and it is not an aerodynamic lens. A laminar flow window is formed by two opposite gas flows that meet each other and escape the cell through a narrow gap between the left/right buffer and the central parts of the cell, Fig. 1. Arrows in Fig. 1 show directions of the gas flows.

It consists of three different parts: a high-temperature sample cell with a length of 0.533 m and two "buffer" cold gas parts on the left- and the right-hand sides of the hot sample cell. The buffer parts are filled with a UV/IR-transparent (purge) gas (e.g., N_2), whereas the central sample cell can be filled with the gas under investigation (e.g., N_2+H_2O/CO_2). The aperture of the sample cell is kept small (i.e., a diameter of 0.015 m) in order to reduce heat transfer by radiation from the sample cell and to reduce the risk of collapse of well-defined flows in the laminar flow windows. The laminar flow windows also function as a radiation shield. Similarly, apertures placed at the ends between the laminar flow windows and the cold windows reduce the heat losses by radiation and convection by breaking down the vortices created by the thermal gradient in the buffer sections. High-quality alumina ceramics were used in order to minimize hetero-phase reactions and to avoid contact of the sample gas with any hot metal parts. A uniform temperature profile is obtained by heating the gas cell with a dedicated three-zone furnace in order to compensate for the heat loss at the ends of the gas cell. The sample gas is preheated. Flows of the gases in the sample cell and in the buffer parts are kept at about the same flow rates. The outer windows placed at the ends of the buffer parts are replaceable. In all experiments, KBr-windows have been used. The gas flow through the HGC maintains a highly uniform and stable temperature in the range 23–1500 °C. The temperature uniformity over 0.45 m in the sample cell was found to be better than

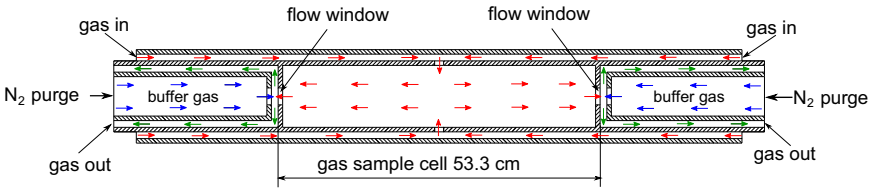

Fig. 1. High-temperature flow gas cell (HGC) used in the experiments [14,16]. Arrows show directions of the gas flows. See text for more explanation.

± 1 °C (the maximum and minimum temperature values T_{max} and T_{min} measured by a calibrated thermocouple along the central zone of the cell show $T_{max}-T_{min} \leq$ 1 °C), or on average ± 0.5 °C.

High-resolution IR-absorption measurements were performed with an FTIR-spectrometer (Nicolet model 5700) equipped with DTGS and InSb IR-detectors. The nominal resolution of the FTIR, $\Delta\eta$, was set to 0.125 cm^{-1} and was sufficient in order to observe in fine-structure absorption band features of CO_2 and H_2O molecules.

A highly stable calibrated blackbody operating at 800 °C was utilized as an IR light source for absorption and reference measurements. After passing through the HGC, the IR light beam was restricted by a variable aperture to minimize possible surface effects from the HGC with another pass through an aperture (Jacquinot-stop) mounted on the outer part of the Nicolet spectrometer operated in the external light source mode. More detail about the experimental setup can be found in [14]. Experiments have been performed with various mixtures of N_2+CO_2 (1–100%) and N_2+H_2O (8–40%) at a flow rate of about 2 l/min. Different CO_2 concentrations were obtained by flow mixing of N_2 with either pre-mixed N_2+CO_2 (1%, 10%) or CO_2 (100%) gases at different N_2:N_2+CO_2 (1%, 10%) or N_2:CO_2 (100%) ratios at temperatures from 1000 K up to 1773 K. Calibrated mass-flow controllers were used to control the gas flows. More detail can be found in [14]. For H_2O IR-absorption measurements an accurate HAMILTON syringe pump system [20] with a water evaporator was used in order to produce controlled N2+H2O (8–40%) mixtures for temperatures up to 1673 K. Transmissivity spectra of CO_2 and H_2O were calculated from four interferograms measured with N_2 and N_2+CO_2 (or H_2O) with and without IR light source as described in [14], Eq. (1). To make these data comparable with Bharadwaj and Modest's experimental transmissivity data and to make the inverse calculation more efficient, the high-resolution data were convolved to medium-resolution (nominal resolution $\Delta\eta = 4\ cm^{-1}$).

In this study, the CO_2 and H_2O transmissivity data measured by Bharadwaj and Modest [12,13,15] with medium-resolution ($\Delta\eta = 4\ cm^{-1}$) at lower temperatures (below 600 K) are used as inputs for the inverse calculation model. For temperatures of 1000 K and beyond, medium-resolution ($\Delta\eta = 4\ cm^{-1}$) data, which are convolved from the high-resolution CO_2 and H_2O transmissivities of Fateev and Clausen's [14,16], are used as inputs. For Bharadwaj and Modest's measurements, the uncertainty in temperature is claimed to be $< 2\%$ at all temperatures. The experimental uncertainty for measurement of CO_2 concentration by the flow meter is 5% of maximum flow meter range [21] (the error can be very high for measuring small CO_2 concentration). The gas chromatograph used for measuring H_2O concentrations is accurate to 5% [15]. In Fateev and Clausen's measurements, temperatures and gas concentrations were claimed very accurate and due to design of the cell and laminar flow arrangement the concentration profile is highly uniform along the cell [22]. However, as shown in Fig. 1, small fluctuations of sample gas path length are also possible due to thermal expansion of the gas cell ceramics with temperature. It is estimated that the optical path length is increased by 0.7 cm or 1.3% when raising the temperature from ambient to 1600 °C [22].

3. Inverse radiation model development

3.1. Forward calculation

A forward calculation model was developed to calculate convolved transmissivities for a given pressure path length, gas concentration and temperature, and was incorporated into the inverse calculation model (see next section) to provide predicted transmissivities. For a homogeneous gas path, the spectral transmissivity is given by

$$\tau(\eta) = e^{-\kappa_\eta L} \tag{1}$$

where κ_η is the absorption coefficient calculated from the HITEMP 2010 LBL database, and L is the gas path length. Since the FTIR measures the spectral transmissivity convolved with an instrument line function (ILF), the LBL spectral transmissivities are also convolved with the ILF. Different FTIR has different ILF, the ILF in the forward calculation model need to be changed accordingly. A Mattson infinity HR series FTIR used by Bharadwaj and Modest uses triangular apodization. In order to use their experimental data to validate the model, the ILF of this FTIR is used in the present study. The Fourier transform (FT) of the triangular apodization function is the instrument line function Γ

$$\Gamma(\eta) = \Delta \mathrm{sinc}^2(\pi\Delta\eta) = \Delta \frac{\sin^2(\pi\Delta\eta)}{(\pi\Delta\eta)^2} \tag{2}$$

where Δ is commonly termed the FTIR retardation.The nominal resolution of an FTIR is generally defined as $1/\Delta$ [23]. Because retardation cannot be infinitely large, FTIRs can only obtain finite resolution and the resolution can be adjusted by changing the retardation of the moving mirror. However, the relationship between retardation and resolution may be defined in different ways [24]. A Mattson infinity HR series FTIR used by Bharadwaj and Modest [12,13,15] has a retardation of $\Delta = 0.666/Res$ and the ILF of this FTIR is used in the present study to compare against Bharadwaj and Modest's measurements, as well as convolved medium-resolution data from Fateev and Clausen's transmissivity measurements. Then Eq. (2) becomes

$$\Gamma(\eta) = \frac{0.666}{Res} \mathrm{sinc}^2\left(\frac{0.666\pi}{Res}\eta\right) \tag{3}$$

After transmissivity spectra are convolved with the ILF $\Gamma(\eta)$, they become

$$\tau_c(\eta) = \int_0^\infty \tau(\eta')\Gamma(\eta-\eta')\,d\eta' \tag{4}$$

As the convolution theorem states, the convolution of two functions equals the inverse Fourier transform of the product of the Fourier transforms of the two functions, or

$$\tau_c(\eta) = \mathcal{F}^{-1}[\mathcal{F}(\tau)\cdot\mathcal{F}(\Gamma)] \tag{5}$$

3.2. Inverse calculation

The present study is limited to homogeneous gas layers of a N_2+CO_2 or N_2+H_2O mixtures and, therefore, only two parameters need to be determined, temperature T and concentration x. Deducing T and x from Eq. (4) requires

deconvolution and makes this problem ill-posed. So instead of directly solving Eq. (4), we do an optimization and retrieve temperature and concentration out of the measured data. By minimizing an objective function, gas temperature and concentration will be deduced. The objective function represents the difference between the predicted and measured transmissivities, i.e.,

$$F = \sum_{i=1}^{I} \left(\frac{\tau_i - Y_i}{\sigma_i} \right)^2 = F\left(\vec{a}\right) \tag{6}$$

where τ_i is the predicted transmissivity spectrum from forward calculations, Y_i is the measured transmissivity spectrum, σ_i^2 is the experimental uncertainty of the data points and $\vec{a} = (x, T)^T$ is the parameter vector. The goal of inverse calculations is to minimize this function by properly guessing the parameter vector until the best match between the measured transmissivity spectrum Y_i and the predicted transmissivity spectrum τ_i is achieved. In the present study, the Levenberg–Marquardt method is applied in the inverse radiation calculations. In this method, the parameter vector $\vec{a}$ is gradually increased by a small value $\vec{\delta a}$

$$\vec{a}_{new} = \vec{a}_{old} + \delta\vec{a} \tag{7}$$

with

$$\delta\vec{a} = -H'^{-1}B \tag{8}$$

and the vector $B = \nabla F(\vec{a})$ is the gradient vector of F with respect to $\vec{a}$, and H' is a matrix with elements

$$h'_{ij} = \begin{cases} (1+\lambda)h_{ij}, & i = j \\ h_{ij}, & i \neq j \end{cases} \tag{9}$$

where the h_{ij} are the elements of the Hessian matrix $H = \nabla^2 F(\vec{a})$.

The nonnegative scaling factor, λ, is adjusted at each iteration. If reduction of the objective function is rapid, a smaller value can be used, whereas if an iteration gives insufficient reduction, λ can be increased. If $\delta\vec{a}$ gets sufficiently small, the iteration will stop and the parameter vector $\vec{a}$ will be obtained. The Levenberg–Marquardt method increases the value of each diagonal term of the ill-conditioned Hessian matrix H (regularization), to mitigate the ill-posedness of the problem. The computational algorithm using the Levenberg–Marquardt method can be summarized as follows [19]:

1. Assume a starting point $\vec{a}_0$.
2. Compute objective function $F(\vec{a}_0)$.
3. Pick a safe (relatively large) value for λ.
4. Solve $\delta\vec{a}$ using Eq. (8).
5. If $F(\vec{a}+\delta\vec{a}) \geq F(\vec{a})$, increase λ, go back to 4.
6. If $F(\vec{a}+\delta\vec{a}) < F(\vec{a})$, decrease λ, update $\vec{a}$ by $\vec{a}+\delta\vec{a}$ and go back to 4.
7. Stop iteration when $|\delta\vec{a}|$ gets sufficiently small

4. Inverse radiation model validation

The measured transmissivity data were used as an input for inverse calculations to retrieve temperature and concentration of the gas. Measured transmissivity data for CO_2 are at temperatures from 300 K to 1773 K and for H_2O are at temperatures from 600 K to 1673 K (only a few cases will show in the paper). At higher temperatures, transmissivity spectral bands tend to be wider. In order to make spectral intervals to be consistent over temperatures, we use relatively wide spectral intervals for all inverse calculations. For lower temperatures, wide intervals may cover lots of useless points (transmissivities approach unity). A wider spectral interval requires more computational efforts but will not significantly effect the retrieved values for temperature and concentration. The wavenumber interval for the CO_2 4.3 μm band is from 1900 cm^{-1} to 2500 cm^{-1}, for the CO_2 2.7 μm band is from 3200 cm^{-1} to 3900 cm^{-1}, for the H_2O 2.7 μm band is from 2800 cm^{-1} to 4500 cm^{-1} and for the H_2O 1.8 μm band is from 4700 cm^{-1} to 5900 cm^{-1}. In this study, temperature and concentration were retrieved simultaneously. Results indicate that the individual errors for temperature and concentration inversion show very large differences in some cases, so the separated errors for retrieving temperature and concentration are presented. Spectral transmissivity data for a wide range of temperatures and concentrations were used to retrieve temperatures and gas concentrations. The "retrieved" transmissivity spectra were calculated based on the HITEMP 2010 database at the retrieved temperature and concentration, and were compared with the "measured" transmissivity spectra as well as the "nominal" transmissivity data (calculated with the given experimental temperature and gas concentration values).

4.1. Validation for convolution of convolution

Fig. 2 shows spectral transmissivities for a N_2–CO_2 mixture containing 10% CO_2 at 1 bar and a temperature of 1000 K for small part of the 4.3 μm band. As an example, the band with a nominal resolution of 0.125 cm^{-1} exhibits the distinct line

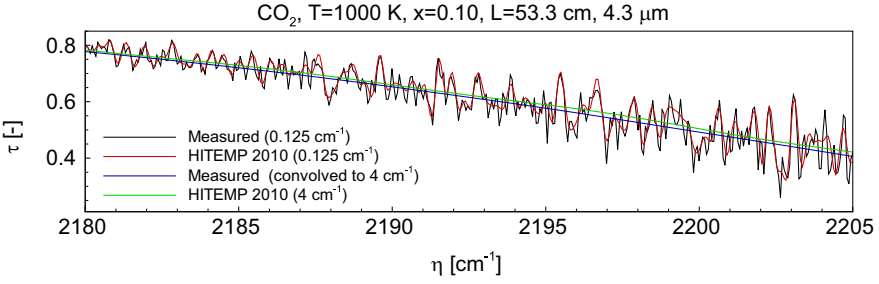

Fig. 2. Comparison of measured transmissivity with calculated transmissivity for lower wavenumber parts of CO_2 (10%) 4.3 μm band at 1000 K.

shape of all stronger lines. While the fine resolution has a very distinct structure, which can be exploited for inversion, it is also subject to theoretical uncertainty, such as calculated values for line strengths, shapes and widths. Fine resolution is also more susceptible to experimental noise, and requires large collection and computational times. After convolving to a medium resolution (here shows 4 cm^{-1}), smoother averaged shapes with less data points are obtained.

The experimental data measured by Fateev and Clausen [14,16] were recorded as interferograms. In order to calculate spectra, an inverse Fourier transform is performed with a certain apodization function. In their experiments, a boxcar apodization function corresponding to a nominal resolution of 0.125 cm^{-1} was used, meaning that the ILF is a *sinc* function. These high-resolution spectra were further convolved with Eq. (3) to convert the spectra into medium-to-coarse resolution data. Accordingly, the forward calculations need to consider the effects of the boxcar apodization function as well as the triangular apodization function. This means Eq. (5) in the forward calculations needs to be changed to

$$\tau_c(\eta) = \mathcal{F}^{-1}[\mathcal{F}(\tau)\cdot\mathcal{F}(\Gamma_1)\cdot\mathcal{F}(\Gamma_2)] \tag{10}$$

where Γ_1 is a *sinc* function with a nominal resolution of 0.125 cm^{-1} and Γ_2 is a $sinc^2$ function with medium-to-coarse nominal resolution, i.e. 1, 2, 4, 8, 16 and 32 cm^{-1}.

It was found that Eqs. (10) and (3) are almost identical for calculating medium-to-coarse resolution transmissivities. Because of the big difference between the nominal resolutions of these two ILFs, as shown in Fig. 3 (a) for the *sinc* function with nominal resolution of 0.125 cm^{-1} and the $sinc^2$ function with nominal resolution of 1 cm^{-1}, the *sinc* function with nominal resolution of 0.125 cm^{-1} has negligible impact on Eq. (10). This can be seen in Fig. 3 (b): the convolution of the two ILFs is almost identical to the $sinc^2$ function with a nominal resolution of 1 cm^{-1}. Very minor differences are observed at the primary peaks and valleys. For other medium-to-coarse resolutions, the differences are even smaller. Therefore, Eq. (3) remains valid for forward calculations.

Table 1 shows the comparison of inverse results using fine-resolution (0.125 cm^{-1}) and medium-to-coarse resolutions (1, 2, 4, 8, 16 and 32 cm^{-1}) transmissivity data for the CO_2 2.7 μm and 4.3 μm bands for temperature and concentration of 1000 K and 0.10, respectively. As shown in the table, the fine-resolution data do not give better results than medium-to-coarse resolution data and the resolutions variation from 1 to 32 cm^{-1} do not have significant effect on the inverse results. Coarse resolutions have fewer data points and require less collection and computational time, so coarse-resolution spectra should be used for optical diagnostics. However, in the present study, the experimental transmissivities measured by Bharadwaj and Modest [12,13,15] have a resolution of 4 cm^{-1}. In order to use these data to validate the model, the resolution of 4 cm^{-1} is used. Accordingly, Fateev and Clausen's experimental transmissivities are convolved to a medium resolution of 4 cm^{-1} to make them comparable with Bharadwaj and Modest's measurements.

4.2. Carbon dioxide

Two CO_2 spectral bands at 2.7 and 4.3 μm were tested at temperature from 300 K to 1773 K. Here we discuss a few examples to show the validity of the inverse model.

First, medium-resolution (4 cm^{-1}) data at lower temperatures for 600 K measured by Bharadwaj and Modest are used. Table 2 and Figs. 4 and 5 show the inverse results and transmissivities comparison for 600 K. The measured data include error bars, which are the experimental standard deviations of six different sets of transmission spectra. For the pure CO_2 case inversion was aided by not allowing unphysical values for concentration. As shown in Fig. 4, there are only small differences between the measured, nominal and retrieved spectra for 2.7 μm band if CO_2 concentration is $x=0.01$, but large errors occur when retrieving CO_2 temperature and concentration. Because the pressure path length (*PxL*) for this case is very small, transmissivities approach unity for large parts of the band and absorption is so weak that the signal-to-noise ratio (SNR) is very small, making the inverse results very sensitives to noise. This may explain why the inverse errors for both temperature and concentration are relatively large. If the pressure path length (*PxL*) increases, the SNR also increases, and errors for temperature and

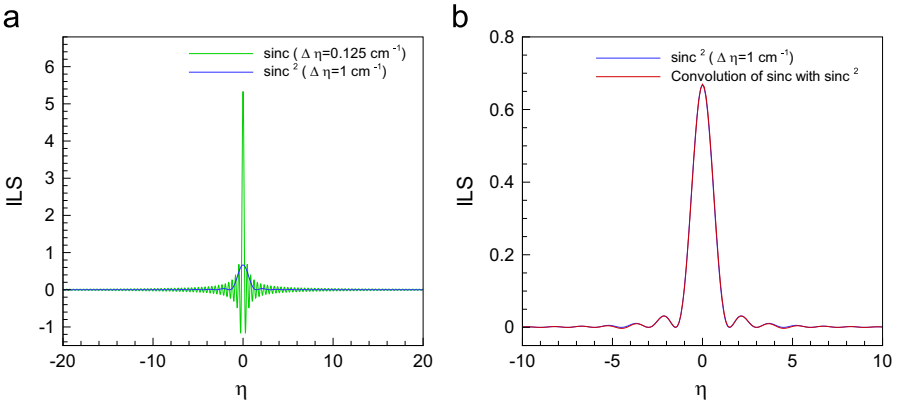

Fig. 3. (a) Comparison of the *sinc* function with nominal resolution of 0.125 cm^{-1} and the $sinc^2$ function with nominal resolution of 1 cm^{-1}. (b) Comparison of convolutions between the two ILFs and $sinc^2$ function with nominal resolution of 1 cm^{-1}.

Table 1
Comparison of inverse calculation results using Fateev and Clausen's transmissivity spectra [14] at fine and medium-to-coarse resolutions for CO_2 at 1000 K and concentration at 0.1.

Test condition (1000 K, 0.10)	Resolution (cm^{-1})	Retrieved T (K)	Retrieved x	Error for T (%)	Error for x (%)
L=53.3 cm, 2.7 μm	0.125	1024.07	0.1072	2.41	7.22
	1	992.32	0.1072	−0.77	7.18
	2	986.97	0.1069	−1.30	6.87
	4	990.84	0.1076	−0.92	7.64
	8	988.17	0.1077	−1.18	7.70
	16	993.96	0.1065	−0.60	6.52
	32	993.31	0.1070	−0.67	6.97
L=53.3 cm, 4.3 μm	0.125	989.07	0.1099	−1.09	9.86
	1	995.36	0.1064	−0.46	6.35
	2	996.24	0.1061	−0.38	6.07
	4	995.48	0.1065	−0.45	6.49
	8	994.17	0.1066	−0.58	6.60
	16	996.30	0.1055	−0.37	5.52
	32	998.46	0.1049	−0.15	4.94

Table 2
Inverse calculation results using Bharadwaj and Modest's transmissivity spectra [12,13] for CO_2 at 600 K.

Test condition (600 K)	Retrieved T (K)	Retrieved x	Error for T (%)	Error for x (%)
L=40 cm, 2.7 μm				
x=0.01	650.36	0.0114	8.39	14.20
x=0.05	607.42	0.0502	1.24	0.44
x=1.00	588.79	1.0000	−1.87	0.00
L=40 cm, 4.3 μm				
x=0.01	587.59	0.0100	−2.07	−0.10
x=0.05	552.75	0.0624	−7.88	24.80
x=1.00	585.65	1.0000	−2.39	0.00

concentration become smaller. Table 2 also includes inverse results for the CO_2 4.3 μm band. It indicates that if the CO_2 2.7 μm band is employed at atmospheric pressure, temperatures and concentrations will be retrieved more accurately for larger concentration, or more importantly, for larger pressure path lengths *PxL*. On the other hand, if the CO_2 4.3 μm is employed at atmospheric pressure, temperatures and concentrations will be retrieved more accurately for a small pressure path length. For the CO_2 4.3 μm band, it is seen that transmissivities tend toward zero for large parts of the band if concentration becomes large enough. Thus, for relatively high CO_2 concentrations, the CO_2 4.3 μm band will not be a good candidate to reconstruct temperatures and concentrations. The large error for small concentrations may well be due to measurement uncertainty of the ball flow meter. Nevertheless, retrieved transmissivities overlap with the measured data very well (as compared to the nominal data) for both bands.

As mentioned before, higher temperature (1000 K, 1473 K, 1550 K, 1773 K) transmissivity data for CO_2 were measured at relatively high-resolution (nominal resolution $\Delta\eta = 0.125\ cm^{-1}$) [14]. Normally the measurements were done twice, and reproducibility was very good (below 0.5%). Baseline stability is about 0.002 [22]. The experimental uncertainties on transmissivity measurements were estimated to be within 5% at a unity transmissivity value [14]. After convolving these data into medium-resolution data, most of the random experimental noise was smoothed out. Examples for two temperatures at 1000 K and 1550 K are shown in Figs. 6–11.

Temperatures are retrieved more accurately than concentrations using the CO_2 2.7 μm or 4.3 μm transmissivity bands at both temperatures, as shown in Tables 3 and 4. For the x=1.00 cases, large differences are observed over the band center between the retrieved transmissivities and the measured one if the CO_2 2.7 μm band is employed, as shown in Figs. 6 and 7. Errors occur when retrieving CO_2 temperature and concentration, but retrieved spectra are in good agreement with measured data for all the cases except for pure CO_2. For pure CO_2, limiting the retrieved concentrations to ≤ 1 makes retrieved temperatures higher than the nominal temperatures. The retrieved concentrations are larger than the nominal concentrations, which may indicate the actual pressure path length *PxL* (probably gas path length *L* due to the "soft" seal for the gas cell) is larger than the nominal pressure path length in the experiments or alternatively, HITEMP 2010 overestimates transmissivity (i.e., underestimates absorption coefficient) in these regions. Two independent measurements from Bharadwaj and Modest [13] and Fateev and Clausen [14] at temperatures 1000 K and 1550 K as shown in Figs. 8 and 9 respectively, both show HITEMP 2010 overestimates transmissivity at the CO_2 2.7 μm band center (Fateev and Clausen's [14] original data have a gas path length of 53.3 cm: in these figures they are scaled to 40 cm and 50 cm accordingly). This indicates that these differences may be caused by incorrectly extrapolated intensities or missing hot lines in the HITEMP 2010 database. For the CO_2 4.3 μm band, although HITEMP 2010 also may overestimate transmissivities at the band center, transmissivities tend toward zero if concentration becomes large enough, which diminishes deviations between measured and nominal transmissivities at the band center. However, the deviations become more significant in the lower wavenumber range for the CO_2 4.3 μm band when temperatures are higher and concentrations are larger. Two independent measurements at 1550 K for pure CO_2 show that HITEMP 2010 may overestimate transmissivity at this temperature also, as shown in Fig. 12, again perhaps due to missing lines or lines with incorrect strength in the database. Due to the fact that all retrieved concentrations are higher than the nominal concentrations and since accurate pre-mixed gases were used with "soft" seals at the ends, the actual gas path lengths may have been higher than 53.3 cm. However, despite measurement errors in the experiments or shortcomings of the database, temperatures can be retrieved fairly accurately and the errors for retrieved temperature are less than 4% for temperatures lower than 1550 K for CO_2.

Although errors occur when retrieving temperature and concentration from measured CO_2 transmissivity spectral data, the retrieved transmissivity spectra are in good agreement with the measured data. The mismatches between the measured and calculated transmissivities based on HITEMP 2010 were identified.

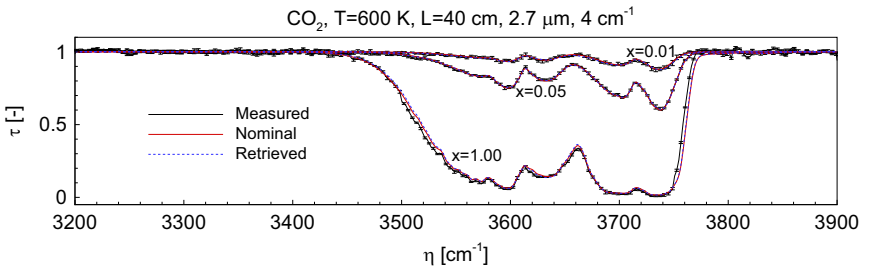

Fig. 4. Comparison of retrieved transmissivity with measured transmissivity [12,13] and nominal transmissivity calculated at the given temperature $T=600$ K for CO_2 2.7 μm band.

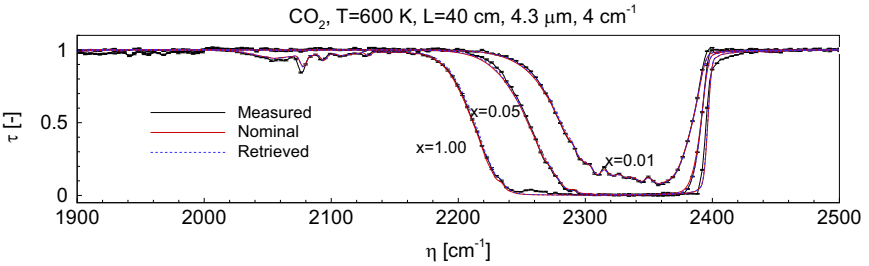

Fig. 5. Comparison of retrieved transmissivity with measured transmissivity [12,13] and nominal transmissivity calculated at the given temperature $T=600$ K for CO_2 4.3 μm band.

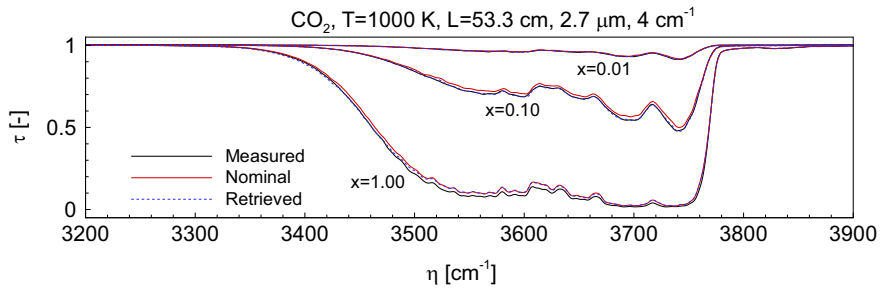

Fig. 6. Comparison of retrieved transmissivity with measured transmissivity [14] and nominal transmissivity calculated at the given temperature $T=1000$ K for CO_2 2.7 μm band.

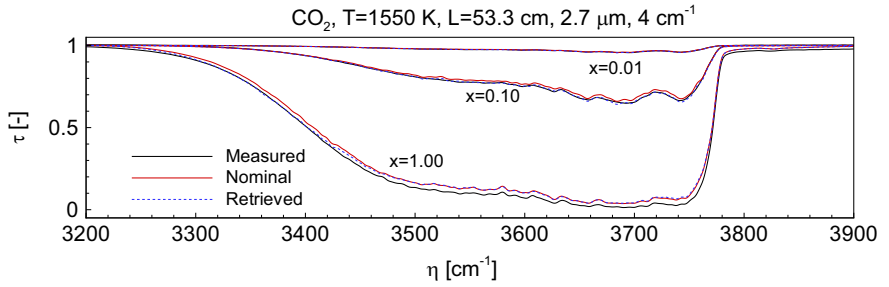

Fig. 7. Comparison of retrieved transmissivity with measured transmissivity [14] and nominal transmissivity calculated at the given temperature $T=1550$ K for CO_2 2.7 μm band.

4.3. Water vapor

Two H_2O spectral bands at 1.8 μm and 2.7 μm were tested using transmissivity data measured by Bharadwaj and Modest [15], and Fateev and Clausen [16] at temperatures from 600 K to 1673 K. Table 5 shows the inverse results at three different temperatures. Here we show the results using medium-resolution ($4\ cm^{-1}$) data at 600 K measured by Bharadwaj and Modest and convolved medium-resolution ($4\ cm^{-1}$) transmissivities from Fateev and Clausen's measurements at 1073 K and 1673 K.

Again, for Bharadwaj and Modest's measurements, the measured data include error bars, which are the experimental standard deviations of six different sets of transmission spectra, as shown in Figs. 13 and 14 for the 1.8 μm and 2.7 μm band, respectively. The retrieved temperatures are

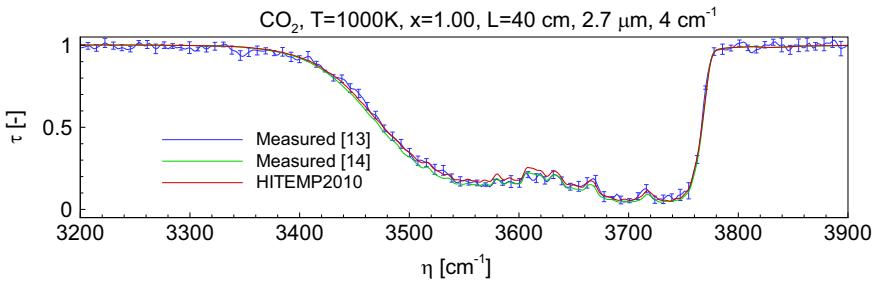

Fig. 8. Comparison of two independently measured transmissivity [13,14] with nominal transmissivity calculated at the given temperature $T=1000$ K for pure CO_2 2.7 μm band.

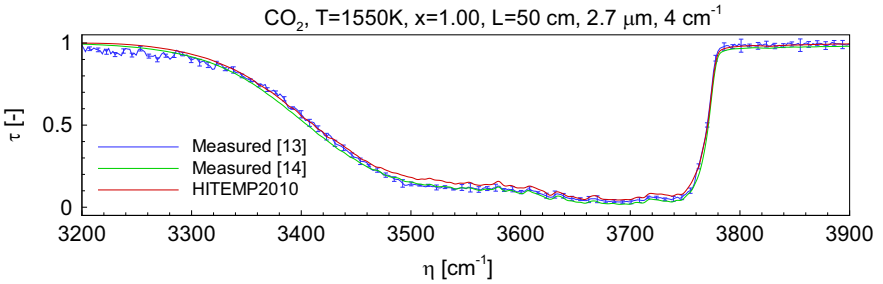

Fig. 9. Comparison of two independently measured transmissivity [13,14] with nominal transmissivity calculated at the given temperature $T=1550$ K for pure CO_2 2.7 μm band.

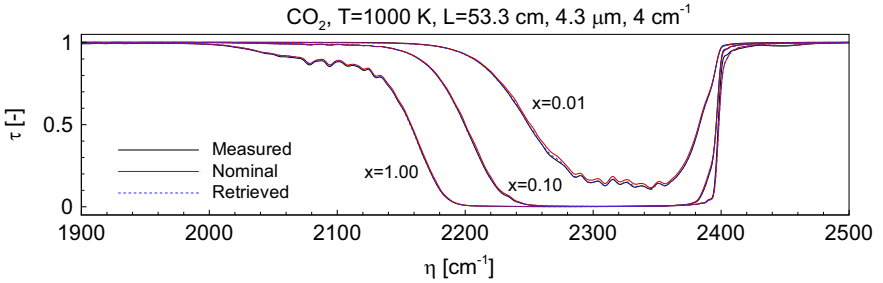

Fig. 10. Comparison of retrieved transmissivity with measured transmissivity [14] and nominal transmissivity calculated at the given temperature $T=1000$ K for CO_2 4.3 μm band.

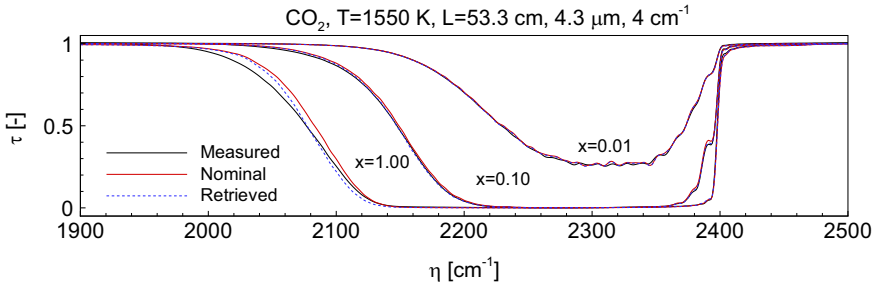

Fig. 11. Comparison of retrieved transmissivity with measured transmissivity [14] and nominal transmissivity calculated at the given temperature $T=1550$ K for CO_2 4.3 μm band.

fairly accurate. For concentration inversion, the measured transmissivities are smaller than the nominal transmissivities for the H_2O 1.8 μm band (as shown in Fig. 13) and limiting the retrieved concentrations to ≤ 1 makes the retrieved concentration to be 1. Still, the retrieved transmissivities do not agree with the measured transmissivities very well. For the H_2O 2.7 μm band, the measured transmissivities are larger than the nominal transmissivities at the band center, which makes the retrieved concentration more than 10% less than unity. Since measured concentrations should be correct for $x=1.00$, possible causes for the deviations include measurement uncertainty of temperatures and/or

total pressures. The measurements were made over a period of 8–12 h for each temperature, the experimental transmissivity in the band is corrected for the drifts of the intensity over time [15]. It is also possible that the wavenumber-based intensity drifts were not appropriately corrected for the band.

Figs. 15 and 16 show the comparison of retrieved transmissivities with measured and nominal transmissivities for H_2O at 1073 K for the 1.8 μm and 2.7 μm bands, respectively. The deviations between nominal and measured transmissivities at temperatures of 1037 K are relatively small and the retrieved temperatures and concentrations are very accurate. Compared to the H_2O 1.8 μm band, the H_2O 2.7 μm band is relatively strong and HITEMP 2010 shows better agreement for this strong band. As shown in Table 5, the retrieved temperatures and concentrations are relatively accurate if using the H_2O 2.7 μm band instead of the 1.8 μm band.

Larger errors for concentration inversions were obtained at the higher temperature of 1673 K; as large as 40% for the H_2O 1.8 μm band and about 20% for the H_2O 2.7 band. At higher temperatures, the deviations become larger both at the band center and band tails, as shown in Figs. 17 and 18. Although it appears to be a baseline offset for the experimental data, careful investigation of high-resolution transmissivity data at 1673 K shows that there is no significant offset for the high-resolution transmissivities. Fig. 19 shows the measured and calculated high-resolution transmissivities at a temperature of 1673 K and H_2O concentration of 0.35 for small parts of the H_2O 1.8 μm band tails and center. The H_2O 1.8 μm band tails are shown in the upper and lower frames in Fig. 19, and the band center is shown in the middle frame. This indicates that the deviations may be caused by HITEMP 2010 failing to describe weak lines in the H_2O band tails and missing hot lines or underestimating line intensities in the band center at higher temperatures. For the two band tails, the measured transmissivities contain a lot of weak H_2O lines which may be missing in the HITEMP 2010 database. Although some of the lines appear to be electronic noise in the measurements, the band tails do contain weak lines. As shown in Fig. 17, after convolving transmissivities into medium resolution, most of the electronic noise is smoothed out, the measured transmissivities are still consistently lower than the calculated transmissivities, which indicates that there are missing weak lines at the band tails in the HITEMP 2010 database. At the band center, it appears that intensities of hot lines are

Table 3
Inverse calculation results using Fateev and Clausen's transmissivity spectra [14] for CO_2 at 1000 K.

Test condition (1000 K)	Retrieved T (K)	Retrieved x	Error for T (%)	Error for x (%)
L=53.3 cm, 2.7 μm				
x=0.01	975.62	0.0102	−2.44	2.30
x=0.10	990.84	0.1076	−0.92	7.64
x=1.00	1026.61	1.0000	2.66	0.00
L=53.3 cm, 4.3 μm				
x=0.01	997.03	0.0106	−0.30	6.10
x=0.10	995.48	0.1065	−0.45	6.49
x=1.00	1005.94	1.0000	0.59	0.00

Table 4
Inverse calculation results using Fateev and Clausen's transmissivity spectra [14] for CO_2 at 1550 K.

Test condition (1550 K)	Retrieved T (K)	Retrieved x	Error for T (%)	Error for x (%)
L=53.3 cm, 2.7 μm				
x=0.01	1545.04	0.0104	−0.32	4.20
x=0.10	1532.24	0.1061	−1.15	6.13
x=1.00	1600.94	1.0000	3.29	0.00
L=53.3 cm, 4.3 μm				
x=0.01	1553.52	0.0101	0.23	1.10
x=0.10	1548.48	0.1066	−0.10	6.57
x=1.00	1610.14	1.0000	3.88	0.00

Table 5
Inverse calculation results using Bharadwaj and Modest's [15] and Fateev and Clausen's [16] transmissivity spectra for H_2O.

Test condition (L=53.3 cm) (μm)	Retrieved T (K)	Retrieved x	Error for T (%)	Error for x (%)
T=600 K, x=1.00 [15]				
1.8	606.67	1.0000	1.11	0.00
2.7	610.89	0.8701	1.81	−12.99
T=1073 K, x=0.35 [16]				
1.8	1117.95	0.3314	4.18	−5.31
2.7	1105.00	0.348	2.97	−0.57
T=1673 K, x=0.35 [16]				
1.8	1751.65	0.5007	4.69	43.05
2.7	1741.38	0.4171	4.08	19.17

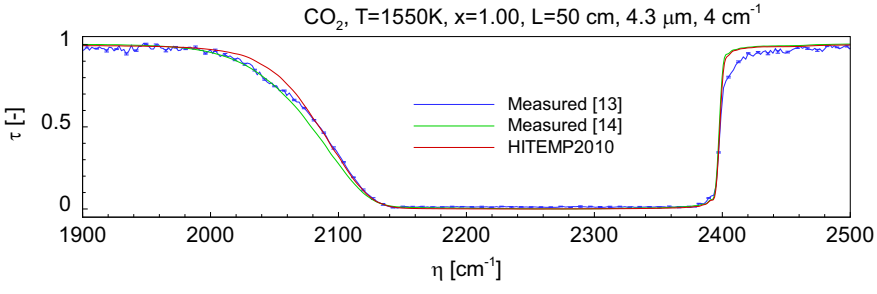

Fig. 12. Comparison of two independently measured transmissivity [13,14] with nominal transmissivity calculated at the given temperature T=1550 K for pure the CO_2 4.3 μm band.

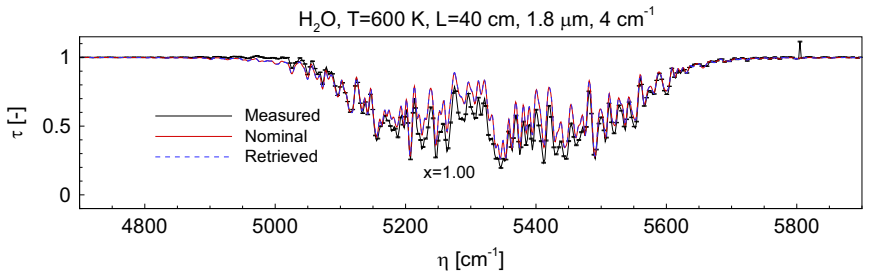

Fig. 13. Comparison of retrieved transmissivity with measured transmissivity [15] and nominal transmissivity calculated at the given temperature $T=600$ K for H_2O 1.8 μm band.

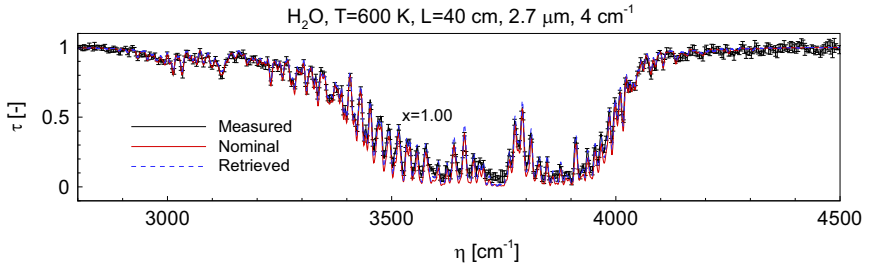

Fig. 14. Comparison of retrieved transmissivity with measured transmissivity [15] and nominal transmissivity calculated at the given temperature $T=600$ K for H_2O 2.7 μm band.

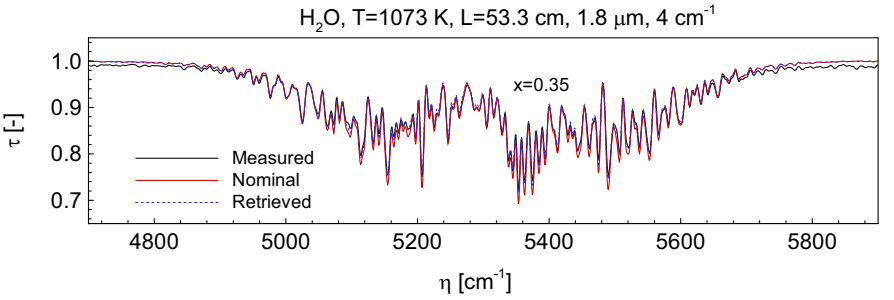

Fig. 15. Comparison of retrieved transmissivity with measured transmissivity [16] and nominal transmissivity calculated at the given temperature $T=1073$ K for H_2O 1.8 μm band.

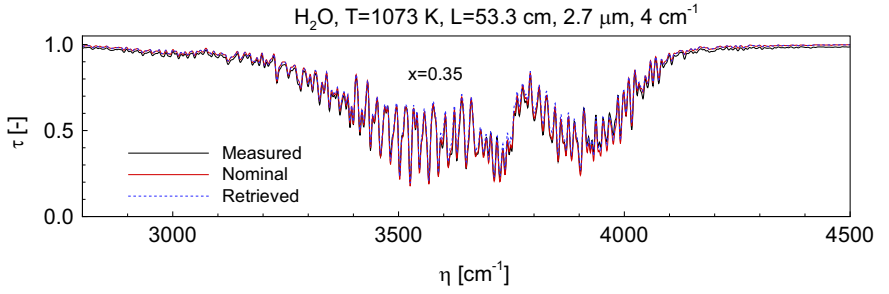

Fig. 16. Comparison of retrieved transmissivity with measured transmissivity [16] and nominal transmissivity calculated at the given temperature $T=1073$ K for H_2O 2.7 μm band.

underestimated, which causes overestimation of transmissivities using the HITEMP 2010 database. This is also observed for the H_2O 2.7 μm band. The deviations can also be caused by introducing errors during the experiments; more measurements at high resolution need to be conducted to validate the HITEMP 2010 database for H_2O spectral calculations at higher temperature, which is beyond the scope of the present study. Although larger errors for

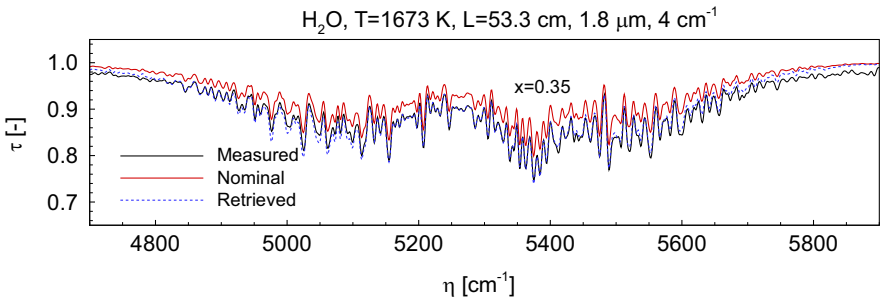

Fig. 17. Comparison of retrieved transmissivity with measured transmissivity [16] and nominal transmissivity calculated at the given temperature $T=1673$ K for H_2O 1.8 μm band.

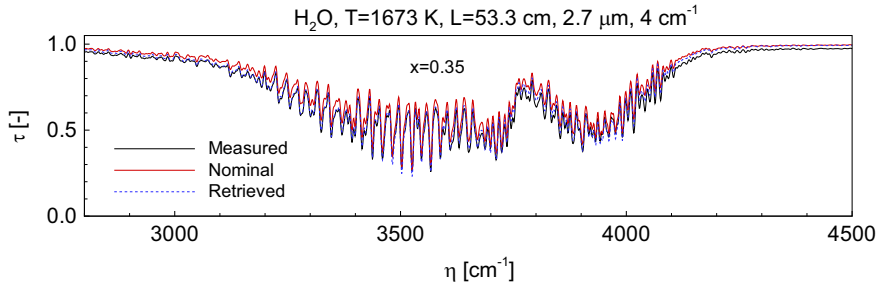

Fig. 18. Comparison of retrieved transmissivity with measured transmissivity [16] and nominal transmissivity calculated at the given temperature $T=1673$ K for H_2O 2.7 μm band.

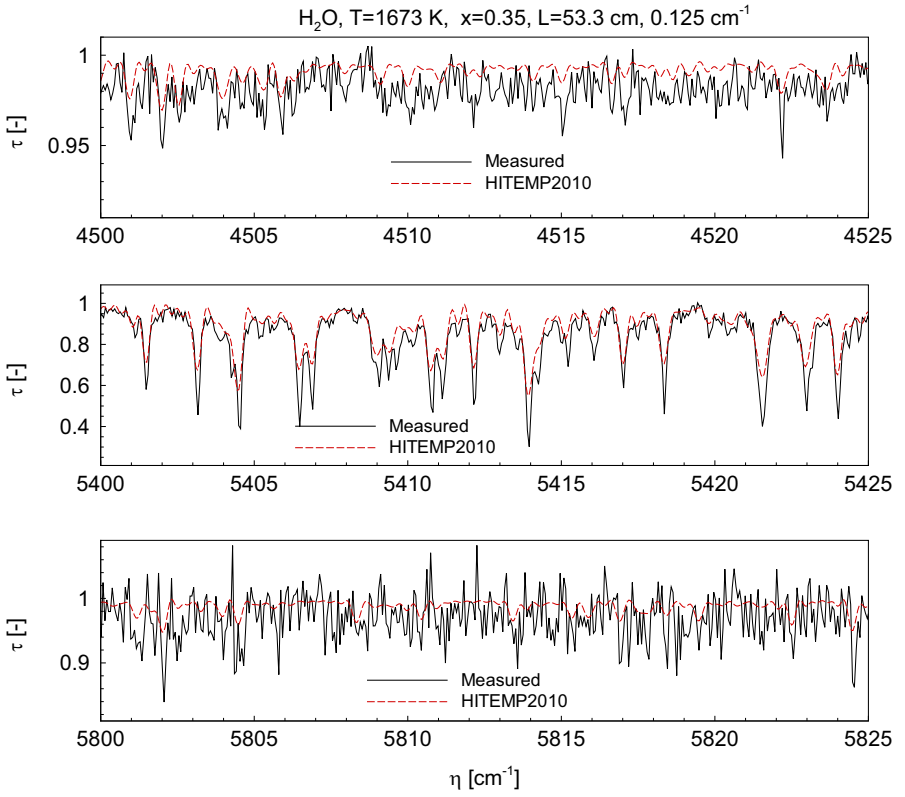

Fig. 19. Comparison of calculated and measured high-resolution (nominal resolution $\Delta\eta=0.125\ \mathrm{cm}^{-1}$) transmissivity [16] at the given temperature $T=1673$ K and concentration $x=0.35$ for H_2O 1.8 μm band.

concentration inversion were obtained for higher temperatures, the retrieved transmissivities always have better agreement with the measured transmissivities.

5. Conclusions

An inverse radiation model was developed by applying the Levenberg–Marquardt scheme for temperature and concentration inversion in combustion gases. The model was validated by retrieving temperatures and gas concentrations using previously measured transmissivity data at a wide range of temperatures and gas concentrations for the CO_2 2.7 μm and 4.3 μm bands and the H_2O 1.8 μm and 2.7 μm bands. The results show that the CO_2 2.7 μm (3200–3900 cm^{-1}) transmissivity band is a good candidate for inverse calculations at larger pressure path lengths, while better temperature and concentration inverse results are obtained if the CO_2 4.3 μm (1900–2500 cm^{-1}) transmissivity band is employed for smaller pressure path lengths. For H_2O, it appears that the HITEMP 2010 database predicts absorption coefficients well up to a temperature of around 1000 K. At higher temperatures HITEMP 2010 may fail to describe weak lines in the band tails and misses hot lines or underestimates line intensities at the band center for the two studied H_2O bands. The results show that the H_2O 2.7 μm transmissivity band is somewhat preferable for retrieving H_2O concentrations. Although the retrieved temperatures and concentrations display large differences compared to the nominal experimental conditions in some cases, good agreement between measured and retrieved transmissivities was observed. The resulting inverse radiation model provides a reliable tool for temperature and concentration prediction.

Acknowledgments

The two primary authors gratefully acknowledge the support from National Science Foundation Grant Nn. CBET-0966627.

References

[1] Rothman LS, Gordon IE, Barber RJ, Dothe H, Gamache RR, Goldman A, et al. HITEMP, the high-temperature molecular spectroscopic database. J Quant Spectrosc Radiat Transf 2010;111(15):2139–50.
[2] Anderson RJ, Griffiths PR. Determination of rotational temperatures of diatomic molecules from absorption spectra measured at moderate resolution. J Quant Spectrosc Radiat Transf 1977;17:393–401.
[3] Gross LA, Griffiths PR. Temperature estimation of carbon dioxide by infrared absorption spectrometry at medium resolution. J Quant Spectrosc Radiat Transf 1988;39(2):131–8.
[4] Solomon PR, Best PE, Carangelo RM, Markham JR, Chien P-L, Santoro RJ, et al. Ft-ir emission/transmission spectroscopy for in situ combustion diagnostics. Proc Comb Inst 1987;21:1763–71.
[5] Best PE, Chien PL, Carangelo RM, Solomon PR, Danchak M, Ilovici I. Tomographic reconstruction of ft-ir emission and transmission spectra in a sooting laminar diffusion flame: species concentrations and temperatures. Combust Flame 1991;85:309–14.
[6] Woo S-W, Song T-H. Measurement of gas temperature profile using spectral intensity from co_2 4.3 μm band. Int J Thermal Sci 2002;41(9):883–90.
[7] Kim HK, Song T-H. Characteristics of srs inversion for measurement of temperature and co_2 concentration profile of a combustion gas layer. J Quant Spectrosc Radiat Transf 2004;86(2):181–99.
[8] Kim HK, Song T-H. Determination of the gas temperature profile in a large-scale furnace using a fast/efficient inversion scheme for the SRS technique. J Quant Spectrosc Radiat Transf 2005;93:369–81.
[9] Song T-H. Spectral remote sensing for furnaces and flames. Heat Transf Eng 2008;29(4):417–28.
[10] Rothman LS, Gordon IE, Barbe A, Benner DC, Bernath PF, Birk M, et al. The HITRAN 2008 molecular spectroscopic database. J Quant Spectrosc Radiat Transf 2009;110:533–72.
[11] Tashkun SA, Perevalov VI. Carbon dioxide spectroscopic databank (CDSD): updated and enlarged version for atmospheric applications, In: Tenth HITRAN conference, Cambridge, MA. Paper T2.3, 2008. Available from: ⟨ftp://ftp.iao.ru/pub/CDSD-2008⟩.
[12] Modest MF, Bharadwaj SP. High-resolution, high-temperature transmissivity measurements and correlations for carbon dioxide–nitrogen mixtures. J Quant Spectrosc Radiat Transf 2002;73(2–5):329–38.
[13] Bharadwaj SP, Modest MF. Medium resolution transmission measurements of CO_2 at high temperature—an update. J Quant Spectrosc Radiat Transf 2007;103:146–55.
[14] Evseev V, Fateev A, Clausen S. High-resolution transmission measurements of CO_2 at high temperatures for industrial applications. J Quant Spectrosc Radiat Transf 2012;113:2222–33.
[15] Bharadwaj SP, Modest MF, Riazzi RJ. Medium resolution transmission measurements of water vapor at high temperature. ASME J Heat Transfer 2006;128:374–81.
[16] Fateev A, Clausen S. On-line non-contact gas analysis. Danmarks Tekniske Universitet, Risø Nationallaboratoriet for Bæredygtig Energi; 2008.
[17] Nocedal J, Wright SJ. Numerical optimization. 2nd ed.Berlin: Springer-Verlag; 2006.
[18] Modest MF. Radiative heat transfer. 3rd ed.New York: Academic Press; 2013.
[19] Press WH, Teukolsky SA, Vetterling WT, Flannery BP. Numerical recipes in FORTRAN—the art of scientific computing. 2nd ed.Cambridge: Cambridge University Press; 1992.
[20] Hamilton Company. URL ⟨http://www.hamiltoncompany.com/item/view/c/785/p/1350/⟩.
[21] Bharadwaj SP. Medium resolution transmission measurements of CO_2 and H_2O at high temperature and a multiscale Malkmus model for treatment of inhomogeneous gas paths [PhD thesis]. The Pennsylvania State University, Department of Mechanical Engineering, University Park, PA; 2005.
[22] Fateev A. Personal communication (2013-12-16).
[23] Griffiths PR, de Haseth JA. Fourier transform infrared spectrometry, chemical analysis.New York: John Wiley & Sons; 1986 Vol. 83.
[24] Reeder TA, Modest MF. Instrument lineshape analysis for a low-resolution FTIR spectrometer. In: Paper no. HT2012-58365. Proceedings of the 2012 ASME summer heat transfer conference, Rio Grande, Puerto Rico; 2012.